The Iron−Sulfur Cluster of Electron Transfer Flavoprotein−Ubiquinone Oxidoreductase Is the Electron Acceptor for Electron Transfer Flavoprotein†

Michael A. Swanson,‡ Robert J. Usselman,‡ Frank E. Frerman,§ Gareth R. Eaton,‡ and Sandra S. Eaton*,‡

Department of Chemistry and Biochemistry, University of Denver, Denver, Colorado 80208, and Department of Pediatrics, University of Colorado School of Medicine, Aurora, Colorado 80045

Received March 24, 2008; Revised Manuscript Received June 19, 2008

ABSTRACT: Electron transfer flavoprotein−ubiquinone oxidoreductase (ETF-QO) accepts electrons from electron transfer flavoprotein (ETF) and reduces ubiquinone from the ubiquinone pool. It contains one $[4Fe\text{-}4S]^{2+,1+}$ and one FAD, which are diamagnetic in the isolated oxidized enzyme and can be reduced to paramagnetic forms by enzymatic donors or dithionite. In the porcine protein, threonine 367 is hydrogen bonded to N1 and O2 of the flavin ring of the FAD. The analogous site in *Rhodobacter sphaeroides* ETF-QO is asparagine 338. Mutations N338T and N338A were introduced into the *R. sphaeroides* protein by site-directed mutagenesis to determine the impact of hydrogen bonding at this site on redox potentials and activity. The mutations did not alter the optical spectra, EPR *g*-values, spin−lattice relaxation rates, or the $[4Fe\text{-}4S]^{2+,1+}$ to FAD point-dipole interspin distances. The mutations had no impact on the reduction potential for the iron−sulfur cluster, which was monitored by changes in the continuous wave EPR signals of the $[4Fe\text{-}4S]^{+}$ at 15 K. For the FAD semiquinone, significantly different potentials were obtained by monitoring the titration at 100 or 293 K. Based on spectra at 293 K the N338T mutation shifted the first and second midpoint potentials for the FAD from +47 and −30 mV for wild type to −11 and −19 mV, respectively. The N338A mutation decreased the potentials to −37 and −49 mV. Lowering the midpoint potentials resulted in a decrease in the quinone reductase activity and negligible impact on disproportionation of ETF_{1e^-} catalyzed by ETF-QO. These observations indicate that the FAD is involved in electron transfer to ubiquinone but not in electron transfer from ETF to ETF-QO. Therefore, the iron−sulfur cluster is the immediate acceptor from ETF.

Electron transfer flavoprotein−ubiquinone oxidoreductase (ETF-QO)[1] is responsible for linking electrons derived from the oxidation of fatty acids and some amino acids to the main mitochondrial respiratory chain (*1*). It is a monotopic membrane protein located on the inner mitochondria membrane facing into the mitochondrial matrix. ETF-QO has two redox-active cofactors, one $[4Fe\text{-}4S]^{2+,1+}$ cluster and one flavin adenine dinucleotide (FAD). ETF-QO oxidizes electron transfer flavoprotein (ETF), a protein responsible for oxidizing nine flavoprotein dehydrogenases and two *N*-methyl dehydrogenases (*2*), and reduces ubiquinone (UQ). UQ then transfers the electrons to the cytochrome bc_1 complex (complex III). Defects in ETF-QO, or its electron donor ETF, result in a metabolic disease known as multiple acyl-CoA dehydrogenase deficiency (MADD) or glutaric acidemia type II (GAII). The severity of this disease depends upon the particular mutation and can range from late-onset in the teenage years to death within the first days after birth (*3, 4*). It is important to understand better the physical properties of this enzyme because of its important role in oxidative metabolism and its link to GAII.

The locations of the redox centers in the crystal structure of porcine ETF-QO provide insights into the possible mechanism of electron transfer in this enzyme (*5*). The FAD molecule is closer to the UQ than the $[4Fe\text{-}4S]^{2+,1+}$ cluster (9.9 Å as opposed to 18.8 Å), and the cluster is closer to the surface of the protein than the flavin ring of FAD (*5*) (Figure 1). This suggests that the $[4Fe\text{-}4S]^{2+,1+}$ cluster is responsible for accepting electrons from ETF and that the FAD is responsible for reducing UQ. The closest approach between the $[4Fe\text{-}4S]^{2+,1+}$ cluster and the FAD is 11.5 Å, which is consistent with electron transfer between the two cofactors (*6*). There is 98% sequence identity between porcine and human ETF-QO and 67% sequence identity between human and *Rhodobacter sphaeroides* ETF-QO (N. J. Watmough, F. E. Frerman, and J. N. Butt, 2008, unpublished results). This high sequence similarity predicts that the tertiary structures are closely related (*7*) and that the mechanism of electron transfer is likely similar in all three enzymes.

Recently, the mutations Y501F, T525A, and Y501F/T525A were introduced into *R. sphaeroides* ETF-QO (*8*). These residues were chosen for mutation because the same

† This work was supported by the National Institutes of Health, Grant NIBIB EB002807 (G.R.E. and S.S.E.), and the Children's Hospital Research Foundation, Denver, CO (F.E.F.).

* Corresponding author. Phone: 303-871-3102. Fax: 303-871-2254. E-mail: seaton@du.edu.

‡ University of Denver.

§ University of Colorado School of Medicine.

[1] Abbreviations: CW, continuous wave; EPR, electron paramagnetic resonance; ETF, electron transfer flavoprotein; ETF-QO, electron transfer flavoprotein−ubiquinone oxidoreductase; FAD, flavin adenine dinucleotide; GAII, glutaric acidemia type II; MADD, multiple acyl-CoA dehydrogenase deficiency; MCAD, medium-chain acyl-CoA dehydrogenase; Q, quinone; Q_1, coenzyme Q_1; QH_2, hydroquinone/quinol; $SQ^{-\bullet}$, anionic semiquinone; UQ, ubiquinone.

10.1021/bi800507p CCC: $40.75
Published on Web 08/02/2008

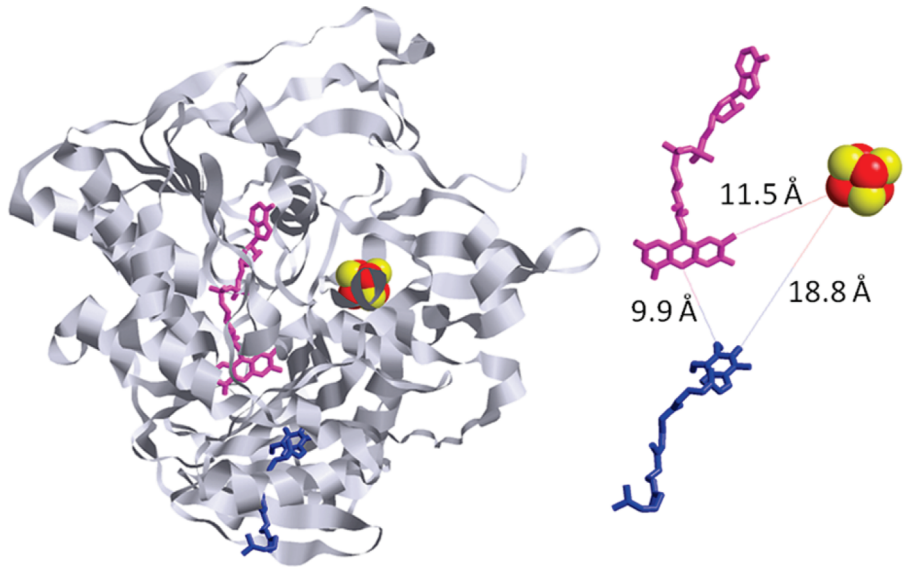

FIGURE 1: Crystal structure of porcine ETF-QO (PDB data bank: 2GMH) highlighting the positions of the three redox centers, [4Fe-4S]$^{2+,1+}$ cluster (red and yellow), FAD (pink), and ubiquinone (blue). On the right the ribbon structure has been removed for clarity, and distances of closest approach of the three redox centers are shown.

residues (although numbered differently) hydrogen bond to the cysteine Sγ atoms that are ligated to the [4Fe-4S]$^{2+,1+}$ cluster of porcine ETF-QO. The mutations eliminate this hydrogen bonding and thus change the redox potential of the [4Fe-4S]$^{2+,1+}$ cluster, which in turn affects the activity of the enzyme. The [4Fe-4S]$^{2+,1+}$ midpoint potentials were lowered by about 100 mV for either single mutation and by about 165 mV for the double mutant. The lower redox potentials of these mutants decreased the quinone reductase activity and the rates of disproportionation of ETF$_{1e^-}$ compared to the wild-type enzyme (*8*). Both single mutations had similar impacts on activities. These results demonstrate that reduction of [4Fe-4S]$^{2+,1+}$ is required for proper enzyme function. As expected, these mutations caused no change in FAD midpoint potentials.

In this study mutations were introduced to modulate the FAD redox potentials and investigate its importance for ETF-QO function. It has been shown that amino acids that form hydrogen-bonding interactions with the isoalloxazine headgroup of a FAD molecule can modulate its redox potentials (*9*). The X-ray crystal structure of porcine ETF-QO (*5*) shows that the location of threonine 367 is suitable for formation of hydrogen bonds with the N1 and O2 of the FAD. In *R. sphaeroides* ETF-QO asparagine 338 is at the position equivalent to threonine 367 of the porcine enzyme. Therefore, it is proposed that this residue is in position to form hydrogen bonds with N1 and O2 of the FAD (Figure 2). The mutations N338A and N338T were introduced to eliminate or lower the energy of the hydrogen bond to the FAD, respectively. The impact of these changes on FAD redox potential and enzyme activity was determined. Results from this study and the previous mutagenesis near the [4Fe-4S]$^{2+,1+}$ cluster can be combined to give a description of the roles of the FAD and [4Fe-4S]$^{2+,1+}$ cluster in ETF-QO electron transfer.

EXPERIMENTAL PROCEDURES

Mutagenesis, Expression, and Purification. The *R. sphaeroides* ETF-QO gene was cloned into the pET21a expression vector, and the wild-type protein was expressed in *Escherichia coli* C43 as previously described (*8*). Site-directed mutagenesis was carried out using the Stratagene QuikChangeII XL site-directed mutagenesis kit. Mutations were confirmed by sequencing. Mutant and wild-type plasmids were transformed into *E. coli* C43 cells (*10*). Cells were grown and protein purified as described previously (*8*). Ubiquinone was not present in the isolated protein. The iron and FAD contents of the enzyme were determined by the methods of Wu et al. (*11*) and Siegel et al. (*12*), respectively. The iron:FAD ratios are 4.0:1 for wild type, 3.6:1 for N338T, and 4.1:1 for N338A.

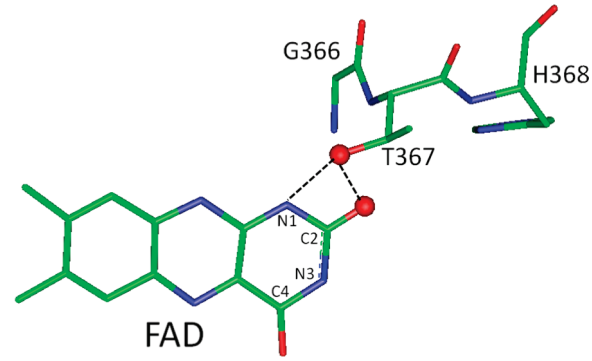

FIGURE 2: Position of threonine 367 and the C2 oxygen of the FAD isoalloxazine group from the porcine ETF-QO crystal structure (PDB data bank: 2GMH). The corresponding amino acid in *R. sphaeroides* ETF-QO is asparagine 338, which is in position to interact with the C2 oxygen and N1 of the isoalloxazine ring.

Enzyme Assays. ETF-QO quinone reductase activity was measured in a coupled reaction containing 10 mM Hepes(K^+) buffer, pH 7.4, 2 μM medium-chain acyl-CoA dehydrogenase (MCAD), 2 μM porcine ETF, 100 μM octanoyl-CoA, 10 mM *n*-dodecyl β-D-maltopyranoside, and 55 μM Q_1 (coenzyme Q_1, Sigma Chemical Co.) at 25 °C (*13*). Q_1 reduction was initiated by the addition of ETF-QO and was monitored by the decrease of absorbance at 275 nm ($\Delta\epsilon = 7.4$ mM^{-1} cm^{-1}).

Disproportionation of ETF$_{1e^-}$ catalyzed by ETF-QO was assayed under anaerobic conditions as described by Beckmann and Frerman (*8, 14*), using 10 μM ETF as substrate.

Reactions were initiated by the addition of ETF-QO, and the decrease in absorbance at 370 nm was monitored. K_m of *R. sphaeroides* ETF-QO is 25 μM so it was impractical to use saturating concentrations of ETF in these assays. However, the assay conditions are satisfactory for comparative purposes because under nonsaturating conditions, the velocity is proportional to the second-order rate constant (*15*).

Spectrophotometric Titrations. Enzymatic reduction of ETF-QO was carried out as reported in ref *8*. Reduction with dithionite was performed on 20 μM ETF-QO in 10 mM Hepes(K^+), pH 7.4, 8 mM CHAPS, and 0.4 mM protocatechuate. The reaction mixtures were made anaerobic by alternate evacuation and purging with argon. Residual O_2 was removed by addition of protocatechuate dioxygenase (*16*). The dioxygenase was a gift from Dr. David Ballou (University of Michigan).

Potentiometric Titrations. Potentiometric titrations of ETF-QO ($\sim$40−100 μM enzyme, 20 mM Hepes (K^+), 20% glycerol (v/v), pH 7.4) using dithionite as reductant were carried out in an anaerobic vessel under continuous N_2(g) flow (*8, 17*).

EPR Spectroscopy. EPR (electron paramagnetic resonance) spectroscopy, signal quantitation, and analysis of the data for $[4Fe\text{-}4S]^+$ at 15 K and for FAD semiquinone ($SQ^{-\bullet}$) at 100 K were done by the methods of Fielding et al. (*18*) for wild-type ETF-QO and Usselman et al. (*8*) for ETF-QO mutants. EPR spectra of FAD $SQ^{-\bullet}$ at 293 K were recorded in 1.0 mm i.d. capillaries on a Varian E9 spectrometer using a microwave power of 0.5 mW, a 2.0 G modulation amplitude, a time constant of 0.25 s, and averaging five 120 s scans. Spectra were quantitated by simulation (*18*) and compared with a tempol (4-hydroxy-2,2,6,6-tetramethylpiperidinooxy) standard.

Relaxation Enhancement Distance Measurements. Enhanced relaxation of the FAD $SQ^{-\bullet}$ signal due to interaction with rapidly relaxing $[4Fe\text{-}4S]^+$ was measured using inversion recovery EPR and was modeled using the locally written program MENOSR, which utilizes a modified version of the Bloembergen equation (*19, 20*). The inversion recovery measurements were performed on samples prepared in the potentiometric titration, selected for the maximum FAD $SQ^{-\bullet}$ signal intensity. The inversion recovery curves are comprised of contributions from FAD $SQ^{-\bullet}$ with neighboring diamagnetic $[4Fe\text{-}4S]^{2+}$ and paramagnetic $[4Fe\text{-}4S]^+$, but only the paramagnetic form of the iron−sulfur cluster enhances the FAD relaxation. In the MENOSR program the distance between the two centers and the fraction of iron−sulfur cluster in the diamagnetic state are both adjusted to give the best fit to the data.

The double mutation Y501F/T525A (*8*), which deletes two hydrogen-bonding interactions with the $[4Fe\text{-}4S]^{2+,1+}$, was used to measure FAD $SQ^{-\bullet}$ relaxation in the absence of enhancement. The $[4Fe\text{-}4S]^+$ midpoint potential for Y501F/T525A ETF-QO is sufficiently low that at −15 mV all of the iron−sulfur cluster is in the diamagnetic +2 oxidation state and does not interact with the FAD $SQ^{-\bullet}$. In the previous study of ETF-QO by Fielding et al. (*18*) the FAD $SQ^{-\bullet}$ in ETF was used to estimate the relaxation rate in the absence of relaxation enhancement. The relaxation rates that were measured for the $SQ^{-\bullet}$ in reduced Y510F/T524A were in good agreement with values obtained previously for the $SQ^{-\bullet}$ in ETF (*8, 18*).

Midpoint Potential Calculations. The relative concentrations of the paramagnetic $[4Fe\text{-}4S]^+$ that are needed for the calculations of the midpoint potentials were based on peak-to-peak signal amplitudes (*8*). Double integration was not used because the signals for $[4Fe\text{-}4S]^+$ and FAD $SQ^{-\bullet}$ overlap. For the $[4Fe\text{-}4S]^+$ titration curves the signal at g_x value was selected for the calculations because it is relatively strong and does not overlap with the resonator background signal that was seen at lower field, overlapping with the g_z value. The g_y value was not used because of the close proximity of the FAD $SQ^{-\bullet}$ signal. The midpoint potentials of the $[4Fe\text{-}4S]^{2+,1+}$ cluster (E_m) were calculated by nonlinear least-squares fitting to plots of [ox]/[red] versus E (mV) using the Nernst equation as described previously (*8, 21*). The Mathcad software package (PTC, Needham, MA) was used to fit the data by manually changing the midpoint potential (E_m) to satisfy a least-squares error constraint. The scatter in the data points determines the uncertainty in E_m, which is estimated as about ±5 mV. The first (E_{m1}) and second (E_{m2}) reduction potentials for the FAD were calculated by nonlinear least-squares fitting to plots of [$SQ^{-\bullet}$] versus E (mV) using the Nernst equation. The solver function in Microsoft Excel was used to vary the E_{m1} and E_{m2} values until a minimum sum of squares error between the data points and Nernst equation was found. The average of E_{m1} and E_{m2} can be determined with an uncertainty of about ±5 mV. The maximum values of the $SQ^{-\bullet}$ concentrations measured at 293 K are 75% for wild-type, 39% for N338T, and 41% for N338A ETF-QO. These values are higher than those measured at 100 K, which are 53%, 32%, and 35% for wild type, N338T, and N338A, respectively. The separation between the two potentials, $E_{m1} - E_{m2}$, is strongly dependent on the concentration of $SQ^{-\bullet}$ observed at the peak of the titration curve, so the uncertainties in E_{m1} and E_{m2} are estimated as ±15 mV.

Duplicate titrations of wild-type protein were carried out to determine the reproducibility of the experiment. At 293 K the E_{m1} values calculated from the two sets of data were 44 and 49 mV, respectively (an average of about 47 mV). The E_{m2} values were both found to be −30 mV. At 100 K the E_{m1} values were 8 and 3 mV (average of about 6 mV) and the E_{m2} values were −35 and −11 mV (average of −23 mV). A larger variation was observed in the E_{m2} values at 100 K, which is attributed to uncertainties in the calculated concentration of semiquinone at the peak of the titration curve.

RESULTS AND DISCUSSION

Characterization of Mutants. The optical spectrum of oxidized N338A ETF-QO is shown in Figure 3, trace 1. It is made up of overlapping contributions from the $[4Fe\text{-}4S]^{2+,1+}$ and the FAD. The FAD contributes the dominant peaks at 380 and 430 nm, which are similar for the wild type and two mutants. Quantitation of FAD in wild-type ETF-QO and the two mutants demonstrated incorporation of the FAD, and the approximately 4:1 iron:FAD ratios confirm the presence of the $[4Fe\text{-}4S]^{2+,1+}$ cluster.

The $[4Fe\text{-}4S]^{2+,1+}$ cluster and the FAD are diamagnetic in the oxidized as-isolated enzyme but can be reduced to EPR-detectable forms. The continuous wave (CW) EPR spectra of the FAD $SQ^{-\bullet}$ at 100 K in the two mutants are

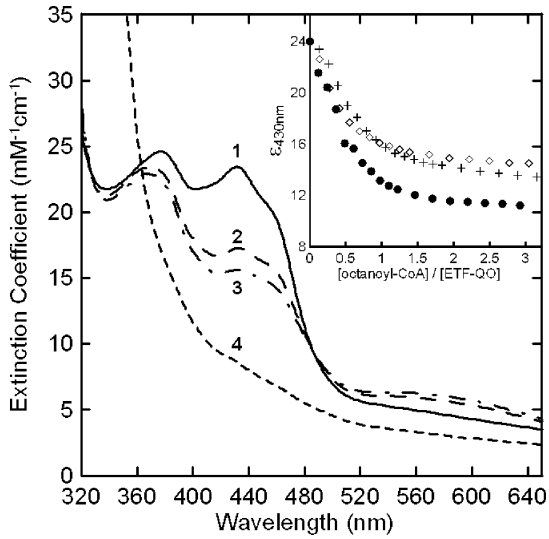

FIGURE 3: Anaerobic reductive titration of N338A ETF-QO. The solution contained 20 μM *R. sphaeroides* N338A ETF-QO, 1.5 μM human ETF, and 0.5 μM human MCAD in 10 mM Hepes(K^+) at pH 7.4. The oxidized sample (spectrum 1) was titrated with octanyl-CoA. After each addition spectra were recorded every 5−10 min until less than 0.001 au change per minute in absorbance was observed. Spectra 2 and 3 correspond to mole ratios of 0.5:1 and 1:1, respectively, and spectrum 4 is the dithionite-reduced enzyme. The inset shows the $\Delta\varepsilon_{430nm}$ vs mole ratio of titrant for (●) wild-type, (+) N338T, and (◇) N338A ETF-QOs.

indistinguishable from those of wild-type protein (Figure 4A). The FAD signal was studied at 100 and 293 K because the relaxation rate of the $[4Fe\text{-}4S]^+$ is so fast at these temperatures that it does not contribute to the CW signal (*18*). The FAD $SQ^{-\bullet}$ signal becomes severely power-saturated at the lower temperatures and higher microwave powers that were used to monitor the $[4Fe\text{-}4S]^+$ signal (*18*). Figure 4B shows the CW spectra of the $[4Fe\text{-}4S]^+$ in the two mutants and wild-type ETF-QO at 15 K. As expected, the $[4Fe\text{-}4S]^+$ line shapes are unchanged by the mutations near the FAD. CW EPR line widths and *g*-values (Table 1) are not changed by mutation.

The temperature dependence of the spin−lattice relaxation rates, $1/T_1$, for $[4Fe\text{-}4S]^+$ at the g_y turning point in the spectrum was measured for the two mutants. Values are the same, within experimental uncertainty, as in the wild-type protein (Figure 5). Analysis of the temperature dependence of the relaxation in terms of contributions from Raman and Orbach process (*18, 22*) showed that the energy of the low-lying excited state, $\Delta E = 210 \pm 5$ K (146 cm^{-1}), is unchanged by the mutations.

Interaction between the rapidly relaxing $[4Fe\text{-}4S]^+$ and the more slowly relaxing FAD $SQ^{-\bullet}$ enhances the electron spin relaxation rate for the $SQ^{-\bullet}$, which can be used to find the point-dipole distance between the two centers (*18, 19*). This method was used to determine a distance of 18.4 Å between the center of the iron−sulfur cluster and the weighted average position of the spin densities of FAD in *R. sphaeroides* ETF-QO (*8, 18*). The inversion recovery curves for the FAD $SQ^{-\bullet}$ signal in the two mutants were modeled using the program MENOSR (*20*). The inversion recovery curves for wild type and N338T were very similar to that for N338A (Figure 6). For the N338T mutation the calculated distance between centers was 17.7 ± 0.9 Å, and the fraction of the cluster in the noninteracting, diamagnetic form was 28 ± 10%. Inversion recovery data for the N338A mutant were in good agreement with a calculated distance of 17.4 ± 0.9 Å and 30 ± 10% noninteracting $[4Fe\text{-}4S]^{2+}$ cluster (Figure 6). The stated errors are standard deviations for results at temperatures between 31 and 50 K. Also shown in Figure 6 is the inversion recovery curve for the double mutant, Y501F/T525A, which lacks relaxation enhancement. The distances in the mutants are slightly smaller than the value of 18.4 Å previously calculated for wild-type ETF-QO. One explanation for this difference could be that the mutants alter the spin density of the FAD $SQ^{-\bullet}$ so that the point dipole is slightly closer to the cluster. The similarities in line shapes of the FAD $SQ^{-\bullet}$ signals (Figure 4A) indicate that any changes in spin density distributions are too small to have large impacts on major hyperfine couplings.

The similarity in CW EPR line shapes and *g*-values, the similarity in optical spectra, the fact that no detectable change in the $[4Fe\text{-}4S]^+$ relaxation times was seen, the observed 4:1 iron to FAD ratios, and the similarity in the distances between the iron−sulfur cluster and the FAD $SQ^{-\bullet}$ radical all suggest that the mutations did not cause major structural changes to the enzyme.

Spectrophotometric Titration. ETF-QO can be reduced either enzymatically using octanoyl-CoA as the electron donor or chemically with dithionite. The extent of reduction can be monitored by changes in the optical spectra (*1, 8, 14, 21*). Figure 3 shows the absorption spectra for oxidized N338A (trace 1), samples reduced with 0.5:1 and 1:1 mol ratios of octanoyl-CoA to ETF-QO (traces 2 and 3, respectively), and with excess dithionite (trace 4). For wild-type ETF-QO these ratios represent roughly 1 and 2 electron-reduced ETF-QO because each mole of octanoyl-CoA can transfer two electrons to the enzyme. The inset in Figure 3 is a plot of the change in ε_{430} as a function of octanoyl-CoA added for wild-type and mutant ETF-QOs. The mutant proteins have higher limiting values for ε_{430} than wild type because octanoyl-CoA is not a strong enough reductant to fully reduce the FAD in the two mutants, with lower E_{m1} compared to wild-type ETF-QO.

Potentiometric Titration. CW EPR signals of FAD $SQ^{-\bullet}$ and $[4Fe\text{-}4S]^+$ were used to monitor the dithionite titrations (Figures 7 and 8). The FAD potentiometric titration curves for wild type and N338T and N338A mutants of *R. sphaeroides* ETF-QO are shown in Figure 7A (titration at 277 K and spectra recorded at 100 K) and Figure 7B (titration at 293 K and spectra recorded at 293 K). The solid lines are least-squares fits of the Nernst equation to the data. Calculated midpoint potentials are shown in Table 2.

The midpoint potentials calculated based on FAD $SQ^{-\bullet}$ spectra recorded at 293 K differed significantly from those calculated from spectra at 100 K. The averages of E_{m1} and E_{m2} determined at 100 K were 16 to 45 mV more negative than at 293 K (Table 2). Differences in reduction potentials determined from EPR spectra at ambient and cryogenic temperatures have been reported previously for other proteins including *Saccharomyces cerevisiae* flavocytochrome b_2 and *E. coli* sulfite reductase (*23, 24*). In the following paragraphs emphasis is placed on potentials determined by measurements at 293 K. At 293 K the N338T and N338A mutations lower E_{m1}, the midpoint potential of the quinone/semiquinone (Q/$SQ^{-\bullet}$) couple from +47 mV for wild type to −11 and −37 mV, respectively. Mutations shift the E_{m2}, the midpoint

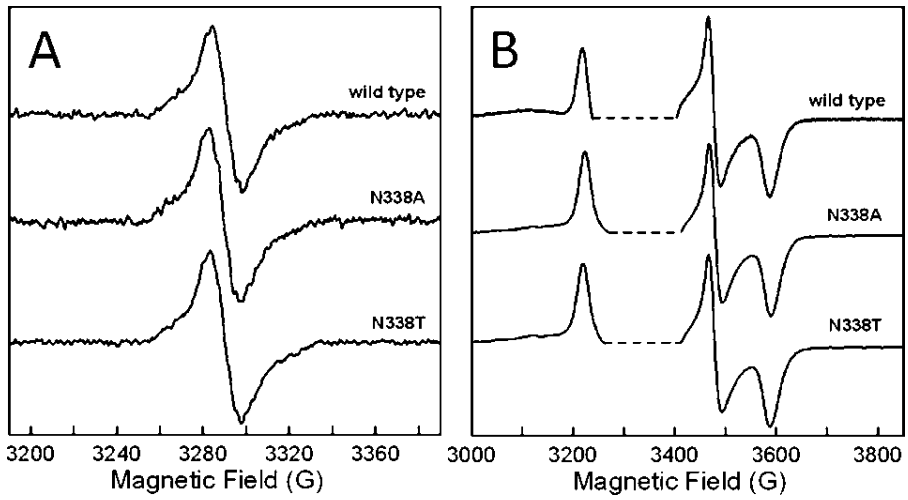

FIGURE 4: X-band CW EPR spectra of *R. sphaeroides* ETF-QO. (A) FAD semiquinone signal recorded at 100 K, 9.23 GHz with 0.01 mW power. A similar line shape, but with lower signal to noise, was observed at 293 K. (B) $[4Fe\text{-}4S]^{+}$ signal recorded at 15 K, 9.35−9.42 GHz with 0.05 mW power. The saturated FAD semiquinone signal was deleted from (B) to aid in comparison (dashed lines). The anaerobic samples contained 20 mM Hepes (K^{+}) and 20% glycerol (v/v) at pH 7.4. Spectra were recorded at their respective maximum semiquinone signals from the potentiometric titrations. The potentials were wild type (−10 mV), N338A (−75 mV), and N338T (−35 mV).

Table 1: *g*-Values[a,b] and Line Widths[c] (G) for $[4Fe\text{-}4S]^{+}$ at 15 K and Semiquinone at 100 K

sample	$[4Fe\text{-}4S]^{+}$ g_z (line width)	$[4Fe\text{-}4S]^{+}$ g_y (line width)	$[4Fe\text{-}4S]^{+}$ g_x (line width)	$SQ^{-\bullet}$ *g*
wild type	2.089 (22)	1.934 (15)	1.875 (29)	2.0036
N338T	2.084 (22.5)	1.930 (17)	1.870 (30.5)	2.0037
N338A	2.084 (22.5)	1.930 (17.5)	1.870 (30.5)	2.0039

[a] The uncertainty of the iron−sulfur cluster *g*-values was ∼±0.003. [b] The uncertainty of the semiquinone *g*-values was ∼±0.0005. [c] Peak-to-peak first derivative line widths were obtained by computer simulation. Uncertainty of the line widths was ±2 G.

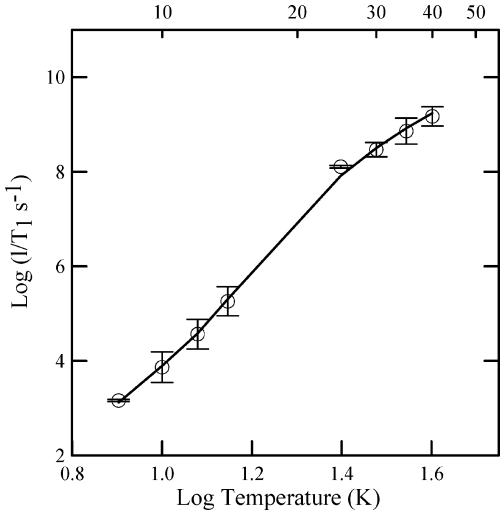

FIGURE 5: Temperature dependence of spin−lattice relaxation rates for dithionite-reduced $[4Fe\text{-}4S]^{+}$ in *R. sphaeroides* ETF-QO. The circles are the average values for wild type, N338T, and N338A mutants. The error bars reflect the standard deviations for the three proteins. The fit line is the sum of contributions from the Raman and Orbach processes. The Debye temperature was fixed at 100 K, and the energy of the low-lying excited state was $\Delta E = 210$ K (146 cm^{-1}).

potential of the semiquinone/quinol ($SQ^{-\bullet}/QH_2$) couple, to −19 and −49 mV for N338T and N338A compared to −30 mV for wild-type ETF-QO.

Figure 8 shows the $[4Fe\text{-}4S]^{2+,1+}$ potentiometric titration curves for the two mutants and wild-type ETF-QO, calculated

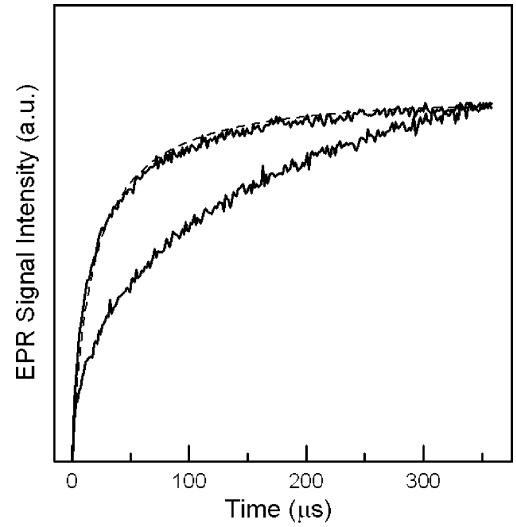

FIGURE 6: Inversion recovery curves for semiquinone in the reduced N338A (upper) and Y501F/T525A (lower) samples of *R. sphaeroides* ETF-QO at 50 K. The samples were produced by reductive titration to the potentials that give the maximum $SQ^{-\bullet}$ signal: N338A (−75 mV) and Y501F/T525A (−10 mV). The curves are the sums of contributions from semiquinone with neighboring diamagnetic $[4Fe\text{-}4S]^{2+}$ and paramagnetic $[4Fe\text{-}4S]^{+}$. The difference between the two curves reflects the impact of the paramagnetic $[4Fe\text{-}4S]^{+}$: N338A (70−80%) and Y501F/T525A (0%). The dashed line is a simulated curve calculated with MENOSR. Simulated curves for both FAD site mutants give an average interspin distance of 17.6 ± 0.9 Å.

from EPR data at 15 K. The low temperature was used because the EPR signal becomes too broad to quantitate at higher temperatures. The E_m of the $[4Fe\text{-}4S]^{2+,1+}$ in the N338T (+48 mV) and N338A (+42 mV) mutants are within experimental uncertainty of the wild-type enzyme (+37 mV). These results show that mutations in the vicinity of the FAD do not impact the redox potentials of the $[4Fe\text{-}4S]^{2+,1+}$. This is consistent with the observation that the $[4Fe\text{-}4S]^{2+,1+}$ site mutations did not impact the redox potentials of the FAD (*8*).

Activity and Disproportionation Assays. The quinone reductase activity assay measures the rate at which electrons are shuttled through the enzyme from its biological electron

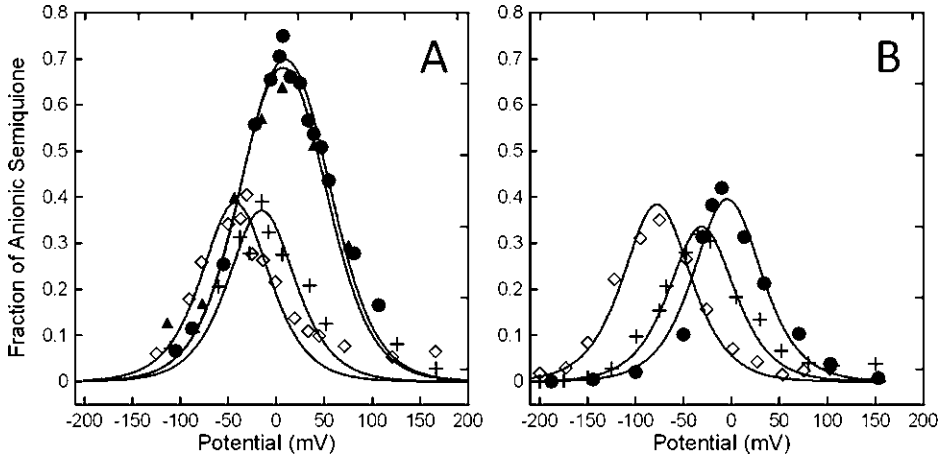

FIGURE 7: Potentiometric titration curves of the FAD semiquinone EPR signals recorded at 293 K (A) and 100 K (B) for *R. sphaeroides* wild-type (●, ▲), N338T (+), and N338A (◇) ETF-QOs. Solid lines are least-squares fitting of the Nernst equation to the data points.

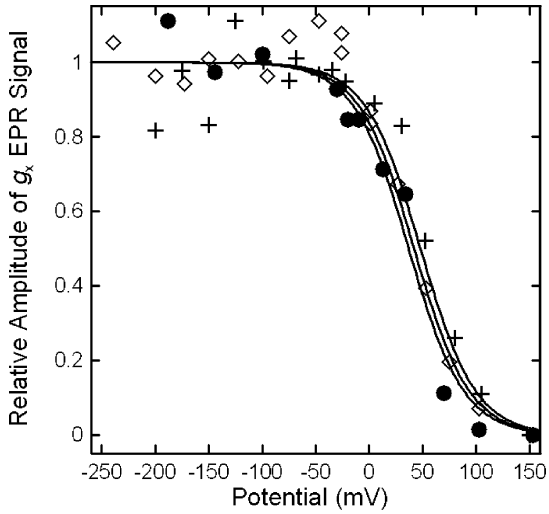

FIGURE 8: Potentiometric titration curves of $[4Fe\text{-}4S]^{+}$ for *R. sphaeroides* wild-type (●), N338T (+), and N338A (◇) ETF-QOs. Data points were based on the X-band g_x EPR signal intensities at 15 K. The midpoint potentials were fit using a single Nernst curve of $n = 1$ (solid lines).

donor, ETF, to its biological electron acceptor, ubiquinone. The relative quinone reductase activities for the N338T, N338A, Y501F, T525A, and Y501F/T525A mutated ETF-QOs are shown in Figure 9A. These values are reported as percents of wild-type activities to facilitate comparisons. Mutations in the vicinity of the $[4Fe\text{-}4S]^{2+,1+}$, Y501F, T525A, and Y501F/T525A, lowered the relative activity to 37%, 35%, and 7% of wild type, respectively. Mutations in the vicinity of the FAD, N338T and N338A, lowered the relative activity to 58% and 35%, respectively (*8*). The differences can be explained by the fact that N338A mutation removes the hydrogen-bonding interaction with the FAD, whereas the N338T mutation only weakens the interaction. More generally it is observed that mutations at both centers decrease the quinone reductase activity. It can be concluded that both the $[4Fe\text{-}4S]^{2+,1+}$ and the FAD are required for full biological function of the enzyme. It can also be concluded that the redox potentials of the two centers are carefully tuned in the wild-type enzyme and that small changes in potentials of one of the centers, such as in the N338T mutant, can cause a substantial decline in the enzyme's activity.

In the disproportionation assay, ETF-QO catalyzes the disproportionation of ETF_{1e^-}, where ETF_{1e^-} serves as both an electron acceptor and donor. Rate constants were measured for the disproportionation of human ETF_{1e^-} by mutant *R. sphaeroides* ETF-QOs and scaled to that for the wild-type enzyme (Figure 9B). The activity, expressed as an average turnover number for wild-type ETF-QO was 8 s^{-1}, which is considerably lower with this heterologous coupled system than the 81.4 s^{-1} for the human ETF and ETF-QO homologue system (*25*). The turnover numbers found previously for the Y501F, T525A, and Y501F/T525A mutants near the iron−sulfur cluster decreased to 4.1, 5.1, and 0.66 s^{-1}, respectively (*8*). These disproportionation rates correspond to roughly 51%, 64%, and 8% of wild-type activity. It is clear that mutations that remove a hydrogen-bonding interaction to the cysteine Sγ ligands of the $[4Fe\text{-}4S]^{2+,1+}$ cluster reduce the rate at which ETF-QO can catalyze the disproportionation of ETF. This is not the case for the N338T and N338A mutations where a slight increase in disproportionation activity was seen. Relative to wild type, the N338A and N338T mutants had roughly 110% activity with rates of 8.8 and 8.9 s^{-1}, respectively. The fact that changing the redox potential of the FAD has no negative effect on catalysis of the disproportionation of ETF $SQ^{-\bullet}$ suggests that the FAD does not directly interact with the ETF. The increase in disproportionation rate in the N338A and N338T mutants could be caused by the lowering of the FAD $Q/SQ^{-\bullet}$ redox potential. Lowering the $Q/SQ^{-\bullet}$ redox potential makes the FAD harder to reduce. The point in the reductive titration curve where $\Delta\varepsilon$ corresponds to the same extent of FAD

Table 2: Midpoint Potentials and Enzymatic Titration $\Delta\epsilon_{430}$ Values for Wild-Type and Mutant ETF-QOs[a]

sample	$[4Fe\text{-}4S]^{2+,1+}$ E_m (mV)	$Q/SQ^{-\bullet}$ E_{m1} (mV)	$SQ^{-\bullet}/QH_2$ E_{m2} (mV)	Q/QH_2 $(E_{m1} + E_{m2})/2$ (mV)	reductive titration $\Delta\epsilon_{430}$
wild type	+37	+47	−30	+8 (+9)	12790
N338T	+48	−11	−19	−15 (−31)	10560
N338A	+42	−37	−49	−43 (−78)	9490

[a] $[4Fe\text{-}4S]^{2+,1+}$ midpoints were measured at 15 K. FAD midpoint potentials were measured at 293 K. Values at 100 K are given in parentheses.

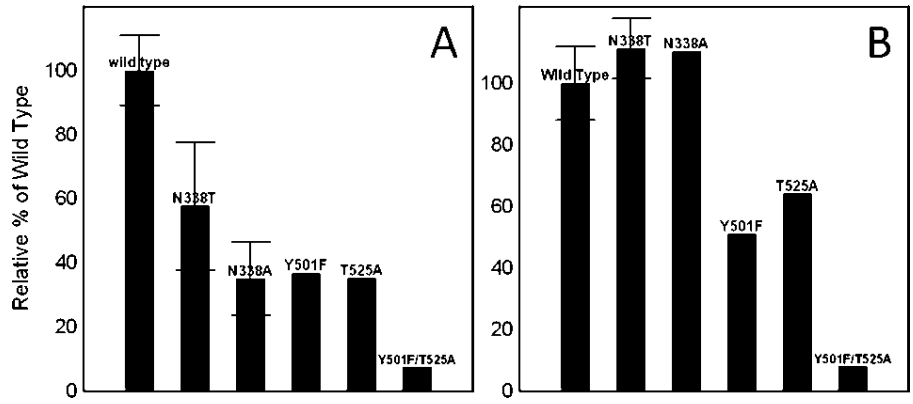

FIGURE 9: Activities of *R. sphaeroides* ETF-QO mutants in (A) quinone reduction and (B) disproportionation of ETF_{1e^-} compared to wild type. Error bars represent the standard deviation between multiple trials.

reduction for the wild-type and mutant proteins is at a lower potential for the mutants. At this potential there is a higher concentration of the $[4Fe\text{-}4S]^+$ form of the cluster, which may enhance interaction with ETF.

Electron Transfer Mechanism. The previous finding that the ubiquinone reductase and disproportionation activities decreased when the midpoint potential of the $[4Fe\text{-}4S]^+$ decreased demonstrates that reduction of the cluster is required for activity. Based on this evidence and the crystal structure of porcine ETF-QO (*26*), it was suggested that electrons from ETF enter ETF-QO through the $[4Fe\text{-}4S]^{2+,1+}$ (*8*). The mutations in the present study shifted the redox potentials of the FAD while leaving the redox potential of the $[4Fe\text{-}4S]^{2+,1+}$ unchanged. The shifted FAD redox potentials cause a decrease in the ubiquinone reductase activity but no decrease in the disproportionation activity. The lower ubiquinone reductase activity suggests that the FAD is required to shuttle electrons through the protein and reduce UQ and is consistent with crystallographic data (*5*). The slight increase in the disproportionation activity suggests that the FAD is not directly involved in the electron transfer between ETF and ETF-QO. Both of these findings support the theory that the electrons are transferred from ETF to ETF-QO through the $[4Fe\text{-}4S]^{2+,1+}$ and then to the FAD which transfers the electrons to UQ as shown in the scheme:

$$\text{ETF} \xrightarrow{e^-} \text{ETF-QO}\ [4Fe\text{-}4S]^{2+} \xrightarrow{e^-}$$

$$\text{ETF-QO (FAD)} \xrightarrow{e^-} \text{ubiquinone}$$

CONCLUSION

The asparagine residue at position 338 of *R. sphaeroides* ETF-QO is postulated to interact with the FAD through hydrogen-bonding interactions. Replacement of the asparagine by threonine lowered E_{m1} by 58 mV and raised E_{m2} by 11 mV. The alanine mutation lowered E_{m1} by 84 mV and E_{m2} by 19 mV compared to wild type. It is proposed that the hydrogen-bonding interaction of the asparagine is completely removed by the alanine mutation but only weakened by the threonine mutation. No change in the midpoint potential of the $[4Fe\text{-}4S]^{2+,1+}$ was detected in these mutants. No evidence of the mutations causing changes in the structure of the enzyme was observed based on the visible and EPR spectra. Quinone reductase activity was lowered by both mutations, demonstrating that reduction of the FAD is required for proper enzyme function. Rates of disproportionation of ETF_{1e^-} were not lowered by the mutations, suggesting that FAD does not interact directly with ETF. These results combined with the previous results for the mutations near the $[4Fe\text{-}4S]^{2+,1+}$ support the proposal that electrons are accepted from ETF through the $[4Fe\text{-}4S]^{2+,1+}$ and are then transferred to FAD which reduces UQ.

REFERENCES

1. Ruzicka, F. J., and Beinert, H. (1977) A new iron-sulfur protein of the respiratory chain: a component of the fatty acid oxidation pathway. *J. Biol. Chem. 252*, 8440–8445.
2. Toogood, H. S., Leys, D., and Scrutton, N. S. (2007) Dynamics driving function—new insights from electron transferring flavoproteins and partner complexes. *FEBS J. 274*, 5481–5504.
3. Goodman, S. I., Binard, R. J., Woontner, M. R., and Frerman, F. E. (2002) Glutaric acidemia type II: gene structure and mutations of the electron transfer flavoprotein ubiquinone oxidoreductase (ETF-QO) gene. *Mol. Genet. Metab. 77*, 86–90.
4. Beresford, M. W., Pourfarzam, M., Turnbull, D. M., and Davidson, J. E. (2006) So doctor, what exactly is wrong with my muscles? Glutaric aciduria type II presenting in a teenager. *Neuromuscular Disord. 16*, 269–273.
5. Zhang, J., Frerman, F. E., and Kim, J.-J. (2006) Structure of electron transfer flavoprotein ubiquinone oxidoreductase and electron transfer to the mitochondrial ubuiquinone pool. *Proc. Natl. Acad. Sci. U.S.A. 103*, 16212–16217.
6. Page, C. C., Moser, C. C., Chen, X., and Dutton, P. L. (1999) Natural engineering principals of electron tunnelling in biological oxidation-reduction. *Nature 402*, 47–52.
7. Chothia, C., and Lesk, A. M. (1986) The relation between the divergence of sequence and structure in proteins. *EMBO J. 5*, 823–826.
8. Usselman, R. J., Fielding, A. J., Frerman, F. E., Eaton, G. R., and Eaton, S. S. (2008) Impact of Mutations on the Midpoint Potential of the $[4Fe\text{-}4S]^+$ Cluster and on the Catalytic Activity in Electron Transfer Flavoprotein-ubiquinone Oxidoreductase (ETF-QO). *Biochemistry 47*, 92–100.
9. Breinlinger, E., Niemz, A., and Rotello, V. M. (1995) Model systems for flavoenzyme activity. Stabilization of the flavin radical anion through specific hydrogen bond interactions. *J. Am. Chem. Soc. 117*, 5379–5380.
10. Miroux, B., and Walker, J. E. (1996) Overproduction of proteins in *Escherichia coli*: mutant hosts that allow synthesis of some membrane proteins and globular proteins at high levels. *J. Mol. Biol. 260*, 289–298.
11. Wu, G., Mansey, S. S., Wu, S., Suresus, K. K., Foster, M. W., and Cowan, J. A. (2002) Characterization of an iron-sulfur cluster assembly protein (ISU1) from *Schizosaccharomyces pombe*. *Biochemistry 41*, 5024–5032.
12. Siegel, L. M. (1978) Quantitative determination of noncovalently bound flavins: types and methods of analysis. *Methods Enzymol. 53*, 419–429.

13. Ramsay, R. R., Steenkamp, D. J., and Husain, M. (1987) Reactions of electron transfer flavoprotein and electron transfer flavoprotein-ubiquinone oxidoreductase. *Biochem. J. 241*, 883–892.
14. Beckmann, J. D., and Frerman, F. E. (1985) Electron transfer flavoprotein-ubiquinone oxidoreductase from pig liver: purification and molecular, redox and catalytic properties. *Biochemistry 24*, 3913–3921.
15. Fersht, A. (1988) in *Structure and Mechanism in Protein Science*, pp 104−105, W. H. Freeman and Co., New York.
16. Patil, P. V., and Ballou, D. P. (2000) The use of protocatechuate dioxygenase for maintaining anaerobic conditions in biochemical experiments. *Anal. Biochem. 286*, 187–192.
17. Dutton, P. L. (1978) Redox potentiomery: determination of mid-point potentials of oxidation reduction components of biological electron transfer systems. *Methods Enzymol. 54*, 411–435.
18. Fielding, A. J., Usselman, R. J., Watmough, N., Simkovic, M., Frerman, F. E., Eaton, G. R., and Eaton, G. R. (2008) Electron Paramagnetic Resonance Characterization and Interspin Distance Measurement of Electron Transfer Flavoprotein Ubiquinone Oxidoreductase (ETF-QO). *J. Magn. Reson. 190*, 222–232.
19. Eaton, S. S., and Eaton, G. R. (2000) Determination of distances based on T_1 and T_m effects. *Biol. Magn. Reson. 19*, 347–381.
20. Rakowsky, M. H., More, K. M., Kulikov, A. V., Eaton, G. R., and Eaton, S. S. (1995) Time-Domain Electron Paramagnetic Resonance as a Probe of Electron-Electron Spin-Spin Interaction in Spin-Labeled Low-Spin Iron Porphyrins. *J. Am. Chem. Soc. 117*, 2049–2057.
21. Paulsen, K. E., Orville, A. M., Frerman, F. E., Lipscomb, J. D., and Stankovich, M. T. (1992) Redox properties of electron-transfer flavoprotein ubiquinone oxidoreductase as determined by EPR-spectroelectrochemistry. *Biochemistry 31*, 11755–11761.
22. Eaton, S. S., and Eaton, G. R. (2000) Relaxation times of organic radicals and transition metal ions. *Biol. Magn. Reson. 19*, 29–154.
23. Tegoni, M., Silvestrini, M. C., Guigliarelli, B., Asso, M., Brunori, M., and Bertrand, P. (1998) Temperature-jump and potentiometric studies on recombinant wild type and Y143F and Y254F mutants of *Saccharomyces cerevisiae* flavocytochrome b_2: Role of the driving force in intramolecular electron transfer kinetics. *Biochemistry 37*, 12761–12771.
24. Coves, J., Zeghouf, M., Macherel, D., Guigliarelli, B., Asso, M., and Fontecave, M. (1997) Flavin mononucleotide-binding domain of the flavoprotein component of the sulfite reductase from *Escherichia coli*. *Biochemistry 36*, 5921–5928.
25. Simkovic, M., Degala, G. D., Eaton, S. S., and Frerman, F. E. (2002) Expression of human electron transfer flavoprotein-ubiquinone oxidoreductase from a baculovirus vector: kinetic and spectral characterization of the human protein. *Biochem. J. 364*, 659–667.
26. Zhang, J., Frerman, F. E., and Kim, J.-J. (2006) Structure of electron transfer flavoprotein ubiquinone oxidoreductase and electron transfer to the mitochondrial ubuiquinone pool. *Proc. Natl. Acad. Sci. U.S.A. 103*, 16212−16217.

BI800507P